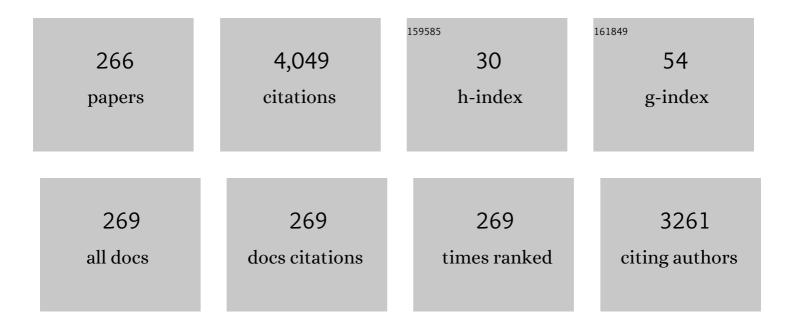
## Qing-An Huang

List of Publications by Year in descending order

Source: https://exaly.com/author-pdf/2704382/publications.pdf Version: 2024-02-01



Οινο-Δν Ημανο

#	Article	IF	CITATIONS
1	Analysis and Compensation of Benchmark Drift of Micromachined Thermal Wind Sensor Caused by Packaging Asymmetry. IEEE Transactions on Industrial Electronics, 2022, 69, 950-959.	7.9	7
2	Simulation and experiment of miniaturized housing structure for MEMS thermal wind sensors. Sensors and Actuators A: Physical, 2022, 333, 113297.	4.1	4
3	Analytic Model of Dual-Layer-Structure MEMS Thermal Wind Sensor With Increased Sensitivity. IEEE Transactions on Electron Devices, 2022, 69, 1341-1348.	3.0	4
4	Passive and Wireless Anemometer Based on Inductor Bending Effect. Journal of Microelectromechanical Systems, 2022, 31, 3-5.	2.5	0
5	A high-throughput microfluidic diploid yeast long-term culturing (DYLC) chip capable of bud reorientation and concerted daughter dissection for replicative lifespan determination. Journal of Nanobiotechnology, 2022, 20, 171.	9.1	5
6	Efficient system-level simulations of thermal wind sensors considering environmental factors. Journal of Micromechanics and Microengineering, 2022, 32, 085002.	2.6	3
7	An efficient <scp>electroâ€thermoâ€mechanical</scp> model for the analysis of Vâ€shaped thermal actuator connected with driven structures. International Journal of Numerical Modelling: Electronic Networks, Devices and Fields, 2021, 34, e2843.	1.9	4
8	Low-Drift MEMS Thermal Wind Sensor With Symmetric Packaging Using Plastic Injection Molding Process. IEEE Transactions on Instrumentation and Measurement, 2021, 70, 1-8.	4.7	6
9	Observation of the perturbed eigenvalues of PT-symmetric LC resonator systems. Journal of Physics Communications, 2021, 5, 045010.	1.2	12
10	Design and 3D modeling investigation of a microfluidic electrode array for electrical impedance measurement of single yeast cells. Electrophoresis, 2021, 42, 1996-2009.	2.4	7
11	Fabrication and Characterization of Flexible Capacitive Humidity Sensors Based on Graphene Oxide on Porous PTFE Substrates. Sensors, 2021, 21, 5118.	3.8	6
12	Flexible LC-Type Wind Speed Sensor With Its Readout Circuit. IEEE Sensors Journal, 2021, 21, 19857-19862.	4.7	1
13	Rotational Speed Measurement Based on LC Wireless Sensors. Sensors, 2021, 21, 8055.	3.8	4
14	Uncertainty quantification of MEMS devices with correlated random parameters. Microsystem Technologies, 2020, 26, 1689-1696.	2.0	4
15	Influence of Aerodynamic Housing on the Performance of MEMS Wind Sensor. , 2020, , .		1
16	A 2D Waveguide Method for Lithography Simulation of Thick SU-8 Photoresist. Micromachines, 2020, 11, 972.	2.9	3
17	Enhancing the Remote Distance of <i>LC</i> Passive Wireless Sensors by Parity-Time Symmetry Breaking. Physical Review Applied, 2020, 13, .	3.8	19
18	Parallelized Wireless Sensing System for Continuous Monitoring of Microtissue Spheroids. ACS Sensors, 2020, 5, 2036-2043.	7.8	11

#	Article	IF	CITATIONS
19	An Impedance Matching Method for LC Passive Wireless Sensors. IEEE Sensors Journal, 2020, 20, 13833-13841.	4.7	9
20	Quadruple sensitivity improvement for wind speed sensor using dual-layer bended inductors. Sensors and Actuators A: Physical, 2020, 303, 111786.	4.1	5
21	Differential piezoresistive wind speed sensor on flexible substrate. Electronics Letters, 2020, 56, 201-203.	1.0	4
22	An efficient macro model for CMOS-MEMS thermal wind speed sensor. Journal of Micromechanics and Microengineering, 2020, 30, 125001.	2.6	4
23	Temperature Effects of a Ceramic MEMS Thermal Wind Sensor Based on a Temperature-Balanced Mode. IEEE Sensors Journal, 2019, 19, 7254-7260.	4.7	9
24	Metal oxide semiconductor nanomembrane–based soft unnoticeable multifunctional electronics for wearable human-machine interfaces. Science Advances, 2019, 5, eaav9653.	10.3	213
25	An Interdigital Capacitive Humidity Sensor With Layered Black Phosphorus Flakes as a Sensing Material. IEEE Sensors Journal, 2019, 19, 11007-11013.	4.7	10
26	Sensitivity Improvement of MEMS Thermal Wind Senor Using Vertical Stacking Thermistors. , 2019, , .		6
27	A Novel Measurement Method of Mechanical Properties for Individual Layers in Multilayered Thin Films. Micromachines, 2019, 10, 669.	2.9	4
28	Ceramic Film Packaging for 2-D Thermal Wind Sensor Using LTCC Technology. Journal of Microelectromechanical Systems, 2019, 28, 1080-1087.	2.5	5
29	Temperature Effect and Its Compensation of a Micromachined 2-D Anemometer. IEEE Sensors Journal, 2019, 19, 5454-5459.	4.7	8
30	Modeling of Packaged MEMS Thermal Wind Sensor Operating on CP Mode. IEEE Transactions on Electron Devices, 2019, 66, 2375-2381.	3.0	6
31	A monolithic integrated ultra-flexible all-solid-state supercapacitor based on a polyaniline conducting polymer. Journal of Materials Chemistry A, 2019, 7, 15378-15386.	10.3	33
32	Fabrication of a Piezoresistive Barometric Pressure Sensor by a Silicon-on-Nothing Technology. Journal of Sensors, 2019, 2019, 1-10.	1.1	5
33	Modeling, Simulation, and Fabrication of a 2-D Anemometer Based on a Temperature-Balanced Mode. IEEE Sensors Journal, 2019, 19, 4796-4803.	4.7	9
34	Novel Anemometer Based on Inductor Bending Effect. Journal of Microelectromechanical Systems, 2019, 28, 321-323.	2.5	9
35	Low Cost Paper-Based LC Wireless Humidity Sensors and Distance-Insensitive Readout System. IEEE Sensors Journal, 2019, 19, 4717-4725.	4.7	32
36	Symmetric LC Circuit Configurations for Passive Wireless Multifunctional Sensors. Journal of Microelectromechanical Systems, 2019, 28, 344-350.	2.5	22

#	Article	IF	CITATIONS
37	Ultra-remote LC Sensor Based on The Broken PT-Symmetry. , 2019, , .		1
38	Implementation of Four-parameter LC Sensing Through Symmetric Dual-Resonant Circuit. , 2019, , .		0
39	Enhancing LC Sensor Telemetry via Magnetic Resonance Coupling. , 2019, , .		1
40	A Fast Response Flexible Humidity Sensor based on PTFE Micropore Substrate. , 2019, , .		1
41	Compact Mems Thermal Wind Sensor Using Dual Polysilicon Layers with Improved Accuracy. , 2019, , .		0
42	Experiments and Solution of Asymmetry Effect for Mems Thermal wind Sensor. , 2019, , .		2
43	Multi-Parameters Detection Implemented by LC Sensors With Branching Inductors. IEEE Sensors Journal, 2019, 19, 304-310.	4.7	11
44	Configuration of a Self-Heated Double Wheatstone Bridge for 2-D Wind Sensors. Journal of Microelectromechanical Systems, 2019, 28, 125-130.	2.5	8
45	Modeling and Simulation of SU-8 Thick Photoresist Lithography. Micro/Nano Technologies, 2018, , 67-97.	0.1	0
46	RF MEMS Switch. Micro/Nano Technologies, 2018, , 1039-1076.	0.1	1
47	Effects of Metal Plane in LC Passive Wireless Sensors. , 2018, 2, 1-3.		9
48	Applying Metamaterial-Based Repeater in LC Passive Wireless Sensors to Enhance Readout. IEEE Sensors Journal, 2018, 18, 1755-1760.	4.7	8
49	A 2D Wind Sensor Using the <inline-formula> <tex-math notation="LaTeX">\$Delta\$ </tex-math> </inline-formula> P Thermal Feedback Control. Journal of Microelectromechanical Systems, 2018, 27, 377-379.	2.5	16
50	Experimental Study of a Dual-Mode Control MEMS Wind Sensor with High Accuracy. , 2018, , .		1
51	Flexible Passive Wireless Pressure and Moisture Dual-Parameter Sensor for Wound Monitoring. , 2018, , .		6
52	Sensitivity Analysis of Micromachined Thermal Wind Sensor Based on Back Surface Sensing Mode. , 2018, , .		3
53	Three-Dimensional Simulation of DRIE Process Based on the Narrow Band Level Set and Monte Carlo Method. Micromachines, 2018, 9, 74.	2.9	6
54	Annular-Encapsulation Packaging to Realize High-Performance MEMS Thermal Wind Sensor. , 2018, , .		3

#	Article	IF	CITATIONS
55	Reliability Optimization of a 3D Packaged Micro-machined Wind Sensor. , 2018, , .		Ο
56	Comprehensive Simulations for Ultraviolet Lithography Process of Thick SU-8 Photoresist. Micromachines, 2018, 9, 341.	2.9	11
57	Encapsulation glue Effect of Encapsulation Glue on Micromachined Thermal Wind Sensor. , 2018, 2, 1-3.		5
58	Readout Distance Enhancement of the Passive Wireless Multi-Parameter Sensing System Using a Repeater Coil. Journal of Sensors, 2018, 2018, 1-6.	1.1	0
59	Octagon-Shaped 2-D Micromachined Thermal Wind Sensor for High-Accurate Applications. Journal of Microelectromechanical Systems, 2018, 27, 739-747.	2.5	18
60	Eight-trigram-inspired MEMS thermal wind sensor with improved accuracy. , 2018, , .		3
61	Experimental Study of the Bending Effect on <italic>LC</italic> Wireless HumiditySensors Fabricated on Flexible PET Substrates. Journal of Microelectromechanical Systems, 2018, 27, 761-763.	2.5	12
62	High-Voltage Flexible Microsupercapacitors Based on Laser-Induced Graphene. ACS Applied Materials & Interfaces, 2018, 10, 26357-26364.	8.0	70
63	LC Wireless Sensitive Pressure Sensors With Microstructured PDMS Dielectric Layers for Wound Monitoring. IEEE Sensors Journal, 2018, 18, 4886-4892.	4.7	57
64	A Micromachined Thermal Wind Sensor. Micro/Nano Technologies, 2018, , 539-576.	0.1	2
65	Micromachined Humidity Sensors. Micro/Nano Technologies, 2018, , 787-816.	0.1	2
66	Modeling and Simulation of Silicon Anisotropic Etching. Micro/Nano Technologies, 2018, , 3-25.	0.1	0
67	Online Test Microstructures of the Thermophysical Properties of MEMS Conducting Films. Micro/Nano Technologies, 2018, , 237-302.	0.1	0
68	Online Test Microstructures of the Mechanical Properties for Micromachined Multilayered Films. Micro/Nano Technologies, 2018, , 197-235.	0.1	0
69	DRIE trenches and full-bridges design for sensitivity improvement of MEMS silicon thermal wind sensor. , 2017, , .		7
70	Experiment of the MEMS Wind Sensor Based on Temperature-Balanced Mode. IEEE Sensors Journal, 2017, 17, 2316-2317.	4.7	10
71	Effects of environmental media on the transmission of an inductive link in wireless microsystems. Frontiers of Mechanical Engineering, 2017, 12, 554-556.	4.3	1
-	DEMENIC Cuttach Tautinglam, 2017 1 20		

72 RF MEMS Switch. Toxinology, 2017, , 1-38.

0.2 1

#	Article	IF	CITATIONS
73	Modelling and characterization of a robust, low-power and wide-range thermal wind sensor. Microsystem Technologies, 2017, 23, 5571-5585.	2.0	4
74	Design and optimization of thermal-mechanical reliability of a TSV 3D Packaged Thermal Wind Sensor. , 2017, , .		1
75	DRIE Trenches and Full-Bridges for Improving Sensitivity of 2-D Micromachined Silicon Thermal Wind Sensor. Journal of Microelectromechanical Systems, 2017, 26, 1073-1081.	2.5	42
76	Towards an LC passive wireless sensor platform. , 2017, , .		0
77	A Micro-Test Structure for the Thermal Expansion Coefficient of Metal Materials. Micromachines, 2017, 8, 70.	2.9	3
78	Modeling of the Effect of Process Variations on a Micromachined Doubly-Clamped Beam. Micromachines, 2017, 8, 81.	2.9	4
79	A Simple Extraction Method of Young's Modulus for Multilayer Films in MEMS Applications. Micromachines, 2017, 8, 201.	2.9	11
80	Micromachined Humidity Sensors. Toxinology, 2017, , 1-30.	0.2	1
81	Effect of Insulation Trenches on Micromachined Silicon Thermal Wind Sensors. IEEE Sensors Journal, 2017, 17, 8324-8331.	4.7	17
82	On-line Test Microstructures of the Mechanical Properties for Micromachined Multilayered Films. Toxinology, 2017, , 1-40.	0.2	0
83	A Generalized Polynomial Chaos-Based Approach to Analyze the Impacts of Process Deviations on MEMS Beams. Sensors, 2017, 17, 2561.	3.8	8
84	Modeling and Simulation of SU-8 Thick Photoresist Lithography. Toxinology, 2017, , 1-31.	0.2	1
85	Online Test Microstructures of the Thermophysical Properties of MEMS Conducting Films. Toxinology, 2017, , 1-67.	0.2	Ο
86	A Micromachined Thermal Wind Sensor. Toxinology, 2017, , 1-43.	0.2	1
87	Modeling and Simulation of Silicon Anisotropic Etching. Toxinology, 2017, , 1-23.	0.2	0
88	In-Situ Testing of the Thermal Diffusivity of Polysilicon Thin Films. Micromachines, 2016, 7, 174.	2.9	1
89	Passive Wireless Hermetic Environment Monitoring System for Spray Painting Workshop. Sensors, 2016, 16, 1207.	3.8	4
90	Parallel capacitive temperature microâ€sensor for passive wireless sensing applications. Electronics Letters, 2016, 52, 1345-1347.	1.0	5

#	Article	IF	CITATIONS
91	An <italic>LC</italic> Passive Wireless Multifunctional Sensor Using a Relay Switch. IEEE Sensors Journal, 2016, 16, 4968-4973.	4.7	19
92	<italic>LC</italic> Passive Wireless Sensors Toward a Wireless Sensing Platform: Status, Prospects, and Challenges. Journal of Microelectromechanical Systems, 2016, 25, 822-841.	2.5	177
93	A Cyclic Scanning Repeater for Enhancing the Remote Distance of LC Passive Wireless Sensors. IEEE Transactions on Circuits and Systems I: Regular Papers, 2016, 63, 1426-1433.	5.4	17
94	A Passive Wireless Adaptive Repeater for Enhancing the Readout of LC Passive Wireless Sensors. IEEE Microwave and Wireless Components Letters, 2016, 26, 543-545.	3.2	63
95	A New Method for Real-Time Measuring the Temperature-Dependent Dielectric Constant of the Silicone Oil. IEEE Sensors Journal, 2016, 16, 8792-8797.	4.7	8
96	Sensitivity Improvement of a 2D MEMS Thermal Wind Sensor for Low-Power Applications. IEEE Sensors Journal, 2016, 16, 4300-4308.	4.7	23
97	A high linearity capacitive temperature sensor fabricated by metalmumps process. , 2016, , .		1
98	A robust and low-power 2-D thermal wind sensor based on a glass-in-silicon reflow process. Microsystem Technologies, 2016, 22, 151-162.	2.0	8
99	Temperature Effects on the Wind Direction Measurement of 2D Solid Thermal Wind Sensors. Sensors, 2015, 15, 29871-29881.	3.8	10
100	An <italic>LC</italic> -Type Passive Wireless Humidity Sensor System With Portable Telemetry Unit. Journal of Microelectromechanical Systems, 2015, 24, 575-581.	2.5	101
101	Three-dimensional simulation of surface topography evolution in the Bosch process by a level set method. Microsystem Technologies, 2015, 21, 1587-1593.	2.0	1
102	Effect of packaging asymmetry on the performance of a 2D MEMS thermal wind sensor with different heating geometries. , 2015, , .		2
103	Temperature dependence of the quality factor in LC-type passive wireless temperature sensors. , 2015, , .		2
104	A new method for measuring the temperature-dependent dielectric constant of the PDMS fluids. , 2015, , .		0
105	Simultaneous Remote Sensing of Temperature and Humidity by LC-Type Passive Wireless Sensors. Journal of Microelectromechanical Systems, 2015, 24, 1117-1123.	2.5	103
106	Laterally-actuated inside-driven RF MEMS switches fabricated by a SOG process. Journal of Micromechanics and Microengineering, 2015, 25, 065007.	2.6	10
107	Implementation of Multiparameter Monitoring by an <italic>LC</italic> -Type Passive Wireless Sensor Through Specific Winding Stacked Inductors. IEEE Internet of Things Journal, 2015, 2, 168-174.	8.7	36
108	Development of a self-packaged 2D MEMS thermal wind sensor for low power applications. Journal of Micromechanics and Microengineering, 2015, 25, 085011.	2.6	26

#	Article	IF	CITATIONS
109	Modeling of Temperature Effects on Micromachined Silicon Thermal Wind Sensors. Journal of Microelectromechanical Systems, 2015, 24, 2033-2039.	2.5	21
110	Development of a robust 2-D thermal wind sensor using glass reflow process for low power applications. , 2015, , .		3
111	A self-packaged self-heated thermal wind sensor with high reliability and low power consumption. , 2015, , .		3
112	Effects of thermally induced packaging stress on a distributed RF MEMS phase shifter. Microsystem Technologies, 2015, 21, 869-874.	2.0	5
113	A self-packaged two-dimensional thermal wind sensor based on thermopiles for low cost applications. Journal of Micromechanics and Microengineering, 2014, 24, 075008.	2.6	5
114	Passive wireless integrated humidity sensor based on dualâ€layer spiral inductors. Electronics Letters, 2014, 50, 1287-1289.	1.0	61
115	Large scale three-dimensional simulations for thick SU-8 lithography process based on a full hash fast marching method. Microelectronic Engineering, 2014, 123, 171-174.	2.4	6
116	Temperature sensing properties of the passive wireless sensor based on graphene oxide films. , 2014, , .		9
117	A novel capacitive temperature sensor for a lab-on-a-chip system. , 2014, , .		6
118	Extending the remote distance of LC passive wireless sensors via strongly coupled magnetic resonances. Journal of Micromechanics and Microengineering, 2014, 24, 125021.	2.6	69
119	Three-dimensional modeling and simulation of the Bosch process with the level set method. , 2014, , .		2
120	Effects of Ambient Humidity on a Micromachined Silicon Thermal Wind Sensor. Journal of Microelectromechanical Systems, 2014, 23, 253-255.	2.5	12
121	Development of a novel bidirectional electrothermal actuator and its application to RF MEMS switch. , 2014, , .		0
122	In-situ determination of the coefficient of thermal expansion of polysilicon thin films using micro-rotating structures. Thin Solid Films, 2014, 552, 184-191.	1.8	6
123	Novel DC-40GHz MEMS series-shunt switch for high isolation and high power applications. Sensors and Actuators A: Physical, 2014, 214, 101-110.	4.1	20
124	2-D Micromachined Thermal Wind Sensors—A Review. IEEE Internet of Things Journal, 2014, 1, 216-232.	8.7	88
125	A simple method for extracting material parameters of multilayered MEMS structures using resonance frequency measurements. Journal of Micromechanics and Microengineering, 2014, 24, 075014.	2.6	11
126	A passive wireless integrated humidity sensor based on dual-layer spiral inductors. , 2014, , .		2

#	Article	IF	CITATIONS
127	Design of LC-type passive wireless multi-parameter sensor. , 2013, , .		7
128	Effect of Environmental Humidity on Dielectric Charging Effect in RF MEMS Capacitive Switches Based on \$C\$– \$V\$ Properties. Journal of Microelectromechanical Systems, 2013, 22, 637-645.	2.5	18
129	MEMS-Based Intraoperative Monitoring System for Improved Safety in Lumbar Surgery. IEEE Sensors Journal, 2013, 13, 1541-1548.	4.7	2
130	Lateral Contact Three-State RF MEMS Switch for Ground Wireless Communication by Actuating Rhombic Structures. Journal of Microelectromechanical Systems, 2013, 22, 10-12.	2.5	19
131	A Novel Three-State RF MEMS Switch for Ultrabroadband (DC-40 GHz) Applications. IEEE Electron Device Letters, 2013, 34, 1062-1064.	3.9	33
132	H2O adsorption-induced curvature of a silicon nanocantilever based on a semi-continuum method. Applied Surface Science, 2013, 282, 662-671.	6.1	3
133	An in-situ measurement method for thermally induced packaging stress in distributed RF MEMS Phase Shifters. , 2013, , .		0
134	Size-dependent thermal expansion properties of Silicon nanowires. , 2013, , .		0
135	Wide span thermal wind sensor system with dual chips. , 2013, , .		0
136	<i>In situ</i> test structures for the thermal expansion coefficient and residual stress of polysilicon thin films. Journal of Micromechanics and Microengineering, 2013, 23, 075019.	2.6	3
137	First-principles study on the electro-mechanical coupling of the Si/Ge core-shell nanowires. , 2013, , .		0
138	Measurement of elastic modulus and residual stress of individual layers for composite films by resonant frequency of MEMS structures. , 2012, , .		0
139	A memory and computation efficient three-dimensional simulation system for the UV lithography of thick SU-8 photoresists. , 2012, , .		1
140	Measurement of material properties for polysilicon thin films by an electrostatic force method. , 2012, , .		1
141	Modeling of H <inf>2</inf> O adsorption-induced curvature of a nanocantilever. , 2012, , .		0
142	Micro-rotating structures for determining thermal expansion coefficients of polysilicon thin films. , 2012, , .		2
143	An online test structure for the thermal expansion coefficient of surface micromachined polysilicon beams by a pull-in approach. Journal of Micromechanics and Microengineering, 2012, 22, 055017.	2.6	4

144 Fabrication of a push-pull type electrostatic comb-drive RF MEMS switch. , 2012, , .

3

#	Article	IF	CITATIONS
145	An equivalent-circuit method for coupled-field modeling of distributed RF MEMS devices and packages. , 2012, , .		1
146	Direct observation of blocked nanoscale surface evaporation on SiO2 nanodroplets. Applied Physics Letters, 2012, 101, 183114.	3.3	1
147	C-V characterization of the piezocapacitive effect with a microfabricated cantilever. , 2012, , .		0
148	Modeling of silicon thermal expansion using strained phonon spectra. Journal of Micromechanics and Microengineering, 2012, 22, 085007.	2.6	8
149	Fullerene as electrical hinge. Applied Physics Letters, 2012, 100, 193111.	3.3	6
150	Gamma and electron beam irradiation effects on the resistance of micromachined polycrystalline silicon beams. Sensors and Actuators A: Physical, 2012, 177, 99-104.	4.1	18
151	Fabrication of a Micromachined Two-Dimensional Wind Sensor by Au–Au Wafer Bonding Technology. Journal of Microelectromechanical Systems, 2012, 21, 467-475.	2.5	59
152	A MEMS pressure sensor based on Hall effect. , 2011, , .		7
153	A hot film wind sensor with four Constant Temperature Difference elements fabricated on ceramic substrate. , 2011, , .		9
154	Humidity sensing properties of the sensor based on graphene oxide films with different dispersion concentrations. , 2011, , .		12
155	Micromachining of Pyrex 7740 Glass by Silicon Molding and Vacuum Anodic Bonding. Journal of Microelectromechanical Systems, 2011, 20, 909-915.	2.5	26
156	A Fully Packaged CMOS Interdigital Capacitive Humidity Sensor With Polysilicon Heaters. IEEE Sensors Journal, 2011, 11, 2986-2992.	4.7	58
157	Enhanced performance of a CMOS interdigital capacitive humidity sensor by graphene oxide. , 2011, , .		24
158	An Efficient Simulation System for Inclined UV Lithography Processes of Thick SU-8 Photoresists. IEEE Transactions on Semiconductor Manufacturing, 2011, 24, 294-303.	1.7	10
159	Modelling of the elastic properties of crystalline silicon using lattice dynamics. Journal Physics D: Applied Physics, 2011, 44, 335401.	2.8	11
160	Theoretical modeling of thermal expansion of crystalline silicon by using the strain phonon spectra. , 2011, , .		0
161	A system level modeling for distributed RF MEMS devices considering thermally induced packaging effect. , 2011, , .		1
162	Wafer level packaging based on AU-AU bonding for a CMOS compatible thermal wind sensor. , 2011, , .		3

#	Article	lF	CITATIONS
163	Gamma Irradiation Effects on Surface-Micromachined Polysilicon Resonators. Journal of Microelectromechanical Systems, 2011, 20, 1071-1073.	2.5	13
164	Complementary metal-oxide semiconductor compatible capacitive barometric pressure sensor. Journal of Micro/ Nanolithography, MEMS, and MOEMS, 2011, 10, 013018.	0.9	2
165	A Modified 3D fast marching simulation for thick photoresists lithography. , 2011, , .		4
166	A hybrid model for the charging process of the amorphous SiO 2 film in radio frequency microelectromechanical system capacitive switches. Chinese Physics B, 2011, 20, 037701.	1.4	2
167	Detecting magnetic field direction by a micro beam operating in different vibration modes. Chinese Physics B, 2011, 20, 097101.	1.4	1
168	Animal experimental study on the nerve root retraction with a silicon pressure sensor. , 2011, , .		1
169	A FCOB packaged thermal wind sensor with compensation. Microsystem Technologies, 2010, 16, 511-518.	2.0	27
170	An electrical probe for measuring thermal expansion coefficients of micromachined polysilicon thin films. , 2010, , .		0
171	Simulations, analysis and characterization of the development profiles for the thick SU-8 UV lithography process. , 2010, , .		1
172	A micromachined silicon capacitive temperature sensor for wide temperature range applications. Journal of Micromechanics and Microengineering, 2010, 20, 055036.	2.6	21
173	A CMOS interdigital capacitive humidity sensor with polysilicon heaters. , 2010, , .		2
174	Elasticity of si calculated with a lattice dynamics model. , 2010, , .		0
175	Micromachining of Pyrex7740 glass and their applications to wafer-level hermetic packaging of MEMS devices. , 2010, , .		8
176	Hot-forming of micro glass cavities for MEMS wafer level hermetic packaging. , 2010, , .		9
177	Design of a capacitive pressure sensor based on flip-chip packaging technology. , 2010, , .		0
178	A Cross-Type Thermal Wind Sensor With Self-Testing Function. IEEE Sensors Journal, 2010, 10, 340-346.	4.7	34
179	Strain Effect of the Dielectric Constant in Silicon Dioxide. Journal of Microelectromechanical Systems, 2010, 19, 1521-1523.	2.5	8
180	A 3D profile simulator for inclined/multi-directional UV lithography process of negative-tone thick photoresists. , 2009, , .		5

#	Article	IF	CITATIONS
181	Orientation Effects in Ballistic High-Strained P-type Si Nanowire FETs. Sensors, 2009, 9, 2746-2759.	3.8	9
182	Modeling and Simulations of Anisotropic Etching of Silicon in Alkaline Solutions with Experimental Verification. Journal of the Electrochemical Society, 2009, 156, F29.	2.9	19
183	A nodal analysis model for the out-of-plane beamshape electrothermal microactuator. Microsystem Technologies, 2009, 15, 217-225.	2.0	4
184	A system-level model for a silicon thermal flow sensor. Microsystem Technologies, 2009, 15, 279-285.	2.0	11
185	Influence of environmental temperature on the dynamic properties of a die attached MEMS device. Microsystem Technologies, 2009, 15, 925-932.	2.0	11
186	A nodal analysis method for electromechanical behavior simulation of bow-tie shaped microbeams. Microsystem Technologies, 2009, 15, 985-991.	2.0	7
187	Pull-in characterization of doubly-clamped composite beams. Sensors and Actuators A: Physical, 2009, 151, 118-126.	4.1	18
188	Modeling of H2O adsorption-induced curvature of a metal/silicon nanocantilever. Applied Surface Science, 2009, 255, 9404-9408.	6.1	8
189	Effect of temperature and elastic constant on the piezoresistivity of silicon nanobeams. Journal of Applied Physics, 2009, 105, 086102.	2.5	10
190	The influence of surface effects on size-dependent mechanical properties of silicon nanobeams at finite temperature. Journal Physics D: Applied Physics, 2009, 42, 045409.	2.8	25
191	Effect of temperature and elastic constant correction on piezoresistivity of silicon nanobeams. , 2009, , .		Ο
192	A Micromachined Inline-Type Wideband Microwave Power Sensor Based on GaAs MMIC Technology. Journal of Microelectromechanical Systems, 2009, 18, 705-714.	2.5	48
193	Effect of Die-Bonding Process on MEMS Device Performance: System-Level Modeling and Experimental Verification. Journal of Microelectromechanical Systems, 2009, 18, 274-286.	2.5	22
194	The effect from the substrate reflection to the inclined UV lithography of SU-8 photoresist. Proceedings of SPIE, 2009, , .	0.8	0
195	Behavior simulation for electrically actuated bow-tie shaped fixed-fixed beams based on nodal analysis method. , 2009, , .		0
196	Analysis of electromagnetic interference of a capacitive RF MEMS switch during switching. Microsystem Technologies, 2008, 14, 349-360.	2.0	8
197	Young's modulus of silicon nanoplates at finite temperature. Applied Surface Science, 2008, 255, 2449-2455.	6.1	20
198	Effect of native oxides on the elasticity of a silicon nano-scale beam. Solid State Communications, 2008, 145, 351-354.	1.9	19

#	Article	IF	CITATIONS
199	Size and temperature dependence of Young's modulus of a silicon nano-plate. Journal Physics D: Applied Physics, 2008, 41, 165406.	2.8	53
200	Flip-chip on board packaging of a thermal wind sensor. , 2008, , .		1
201	Effect of (2 $\tilde{A}$ — 1) Surface Reconstruction on Elasticity of a Silicon Nano-Plate. Chinese Physics Letters, 2008, 25, 1403-1406.	3.3	6
202	Theoretical study of electromechanical property in a p-type silicon nanoplate for mechanical sensors. Chinese Physics B, 2008, 17, 4292-4299.	1.4	5
203	A novel 2-D wind sensor with thermal feedback. , 2008, , .		1
204	Anisotropic etching of silicon in alkaline solutions : Microscopic activation energy calculations for silicon atoms and its simulation applications. , 2008, , .		0
205	Detection of stiction of suspending structures in MEMS by A Laser Doppler Vibrometer systems. , 2008, , .		Ο
206	Modeling and simulation of a novel capacitive temperature sensor. , 2008, , .		0
207	A dynamic macromodel for distributed parameter magnetic microactuators. Chinese Physics B, 2008, 17, 1709-1715.	1.4	4
208	Modeling, simulation and experimental verification of inclined UV lithography for SU-8 negative thick photoresists. Journal of Micromechanics and Microengineering, 2008, 18, 125017.	2.6	23
209	A smart 2-D wind sensor with self-test function. , 2008, , .		1
210	A cellular automaton-based simulator for silicon anisotropic etching processes considering high index planes. Journal of Micromechanics and Microengineering, 2007, 17, S38-S49.	2.6	43
211	Improvement of the 2D dynamic CA method for photoresist etching simulation and its application to deep UV lithography simulations of SU-8 photoresists. Journal of Micromechanics and Microengineering, 2007, 17, 2538-2547.	2.6	53
212	Flip-Chip Packaging for a Two-Dimensional Thermal Flow Sensor Using a Copper Pillar Bump Technology. IEEE Sensors Journal, 2007, 7, 990-995.	4.7	35
213	An atomic level model for silicon anisotropic etching processes: Cellular automaton simulation and experimental verification. Applied Physics Letters, 2007, 91, 174101.	3.3	3
214	A Novel 3-D Dynamic Cellular Automata Model for Photoresist-Etching Process Simulation. IEEE Transactions on Computer-Aided Design of Integrated Circuits and Systems, 2007, 26, 100-114.	2.7	18
215	Package Level Simulation and Verification of Microsystems. , 2007, , .		3
216	A microwave power sensor based on GaAs MMIC technology. Journal of Micromechanics and Microengineering, 2007, 17, 2132-2137.	2.6	27

#	Article	lF	CITATIONS
217	A silicon directly bonded capacitive absolute pressure sensor. Sensors and Actuators A: Physical, 2007, 135, 507-514.	4.1	52
218	In-line method for extracting the temperature coefficient of resistance of surface-micromachined polysilicon thin films. Sensors and Actuators A: Physical, 2007, 136, 249-254.	4.1	5
219	A nodal analysis method for simulating the behavior of electrothermal microactuators. Microsystem Technologies, 2007, 14, 119-129.	2.0	16
220	Numerical study on photoresist etching processes based on a cellular automata model. Science in China Series D: Earth Sciences, 2007, 50, 57-68.	0.9	0
221	An online test microstructure for thermal conductivity of surface-micromachined polysilicon thin films. IEEE Sensors Journal, 2006, 6, 428-433.	4.7	13
222	Coupled Fabrication Process Simulation and Mechanical Performance Analysis of Microstructures Based on Cellular Automata. , 2006, , .		1
223	A new micro-rotating structure. Journal of Physics: Conference Series, 2006, 34, 552-557.	0.4	5
224	Measurement of residual stress in multilayered thin films by a full-field optical method. , 2006, , .		1
225	Measurement of residual stress in multilayered thin films by a full-field optical method. Sensors and Actuators A: Physical, 2006, 126, 93-97.	4.1	13
226	Macro-modeling for polysilicon cascaded bent beam electrothermal microactuators. Sensors and Actuators A: Physical, 2006, 128, 165-175.	4.1	28
227	A modified cellular automata algorithm for the simulation of boundary advancement in deposition topography simulation. Journal of Micromechanics and Microengineering, 2006, 16, 1-8.	2.6	117
228	SPICE Model with Lumped Circuits for A Thermal Flow Sensor. , 2006, , .		2
229	Contact UV Lithography Simulation for Thick SU-8 Photoresist. , 2006, , .		4
230	A Novel Model for Surface Evolvement and Footing Effect Simulations in DRIE Fabrications. , 2006, , .		0
231	Plasma Etching Process Simulation for MEMS and IC Fabrication based on a Cellular Automata Method. , 2006, , .		0
232	A simple method for measuring the thermal diffusivity of surface-micromachined polysilicon thin films. Journal of Micromechanics and Microengineering, 2006, 16, 981-985.	2.6	9
233	Modeling, design and fabrication of a triple-layered capacitive pressure sensor. Sensors and Actuators A: Physical, 2005, 117, 71-81.	4.1	48
234	A novel capacitive pressure sensor based on sandwich structures. Journal of Microelectromechanical Systems, 2005, 14, 1272-1282.	2.5	95

#	Article	IF	CITATIONS
235	A physical model for silicon anisotropic chemical etching. Semiconductor Science and Technology, 2005, 20, 524-531.	2.0	19
236	RF MEMS membrane switches on GaAs substrates for X-band applications. Journal of Microelectromechanical Systems, 2005, 14, 464-471.	2.5	49
237	A novel 2D dynamic cellular automata model for photoresist etching process simulation. Journal of Micromechanics and Microengineering, 2005, 15, 652-662.	2.6	23
238	Large-signal lumped-parameter macromodels for the equivalent circuit representation of electromechanical transducers. Journal of Micromechanics and Microengineering, 2004, 14, 452-461.	2.6	10
239	An analytical model for pull-in voltage of clamped–clamped multilayer beams. Sensors and Actuators A: Physical, 2004, 116, 15-21.	4.1	57
240	A novel capacitive-type humidity sensor using CMOS fabrication technology. Sensors and Actuators B: Chemical, 2004, 99, 491-498.	7.8	128
241	M-Test Method for Measuring Mechanical Property of Multi-layer in MEMS. International Journal of Nonlinear Sciences and Numerical Simulation, 2002, 3, .	1.0	0
242	Numerical simulation of a polysilicon thermal flexure actuator. Microsystem Technologies, 2002, 8, 17-21.	2.0	28
243	An interpretation of reverse current in metal/intrinsic diamond/semiconducting diamond junction diodes. Applied Surface Science, 2001, 171, 57-62.	6.1	4
244	Design and finite element analysis of weighted-stiffness microelectromechanical digital-to-analogue converters. Electronics Letters, 2001, 37, 755.	1.0	9
245	A simple approach to characterizing the driving force of polysilicon laterally driven thermal microactuators. Sensors and Actuators A: Physical, 2000, 80, 267-272.	4.1	27
246	Analytical modeling and optimization for a laterally-driven polysilicon thermal actuator. Microsystem Technologies, 1999, 5, 133-137.	2.0	55
247	Analysis and design of polysilicon thermal flexure actuator. Journal of Micromechanics and Microengineering, 1999, 9, 64-70.	2.6	309
248	An interpretation of SiO2-induced emission instability in silicon field emitter. Applied Surface Science, 1998, 136, 36-40.	6.1	3
249	Field emission from surface states of silicon. Journal of Applied Physics, 1997, 81, 7589-7594.	2.5	16
250	A field-enhanced generation model for field emission from p-type silicon. IEEE Electron Device Letters, 1997, 18, 616-618.	3.9	10
251	Field emission from silicon including continuum energy and surface quantization. Applied Surface Science, 1997, 119, 229-236.	6.1	5
252	Influence of silicon doping density on vacuum field emission triode at high frequency range. Journal of Infrared, Millimeter and Terahertz Waves, 1996, 17, 1447-1456.	0.6	0

#	Article	IF	CITATIONS
253	Analytical piezoelectric charge densities in GaAs MESFETs. IEEE Transactions on Electron Devices, 1996, 43, 509-510.	3.0	Ο
254	Field emission from the surface quantum well of silicon. Applied Surface Science, 1996, 93, 77-83.	6.1	17
255	Instability of field emission from silicon covered with a thin oxide due to electron trapping. Journal of Applied Physics, 1996, 79, 3703-3707.	2.5	16
256	Biasedâ€voltage controlled thinning for bonded siliconâ€onâ€insulator wafers. Applied Physics Letters, 1995, 66, 2990-2991.	3.3	0
257	Field emission from a silicon surface potential well through a thin oxide. Journal of Applied Physics, 1995, 78, 6770-6774.	2.5	13
258	Field emission from a silicon surfaceâ€potential well based on an Airy function approach. Journal of Applied Physics, 1995, 78, 1254-1258.	2.5	6
259	Possible Current Oscillations in Field Emission from N-Type Silicon. Japanese Journal of Applied Physics, 1995, 34, L918-L920.	1.5	2
260	GaAs piezoelectric modulated resistors. Sensors and Actuators A: Physical, 1993, 35, 247-254.	4.1	3
261	A simple C-V method for measuring minority lifetime of nonuniformly doped MOS structures. Solid-State Electronics, 1991, 34, 419-420.	1.4	1
262	A New Interpretation of the Orientation Effect in GaAs Metal Semiconductor Field Effect Transistors. Japanese Journal of Applied Physics, 1991, 30, L11-L14.	1.5	6
263	A novel bonding technology for GaAs sensors. Sensors and Actuators A: Physical, 1990, 21, 40-42.	4.1	3
264	Micro-electro-mechanical digital-to-analog converter based on a novel bimorph thermal actuator. , 0, , .		1
265	On-line extraction for thermal conductivity of surface-micromachined polysilicon thin films. , 0, , .		3
266	An in-situ technique for measuring Young's modulus and residual stress of each layer for multi-layer film. , 0, , .		0